TRACKING PERIODIC PARAMETERS IN THE MEASURED MAGNETIC FIELD MAPS OF A SPIRAL FFAG

S. Antoine, W. Beeckman, F. Forest, J.-L. Lancelot, M.-J. Leray*, F. Méot†

Abstract

Numerical ray-tracing computations in measured field maps have been performed for assessing the qualities of a prototype spiral FFAG magnet that has recently been constructed. Some representative results are presented here.

INTRODUCTION

A prototype of a spiral FFAG lattice magnet has recently been designed [1] and constructed [2], in the frame of the RACCAM project [3], in view of validating

- computational design methods,
- fabrication methods,

by thorough comparison of their respective outcomes.

This prototype is representative of the main dipole of a 10-cell spiral FFAG aimed at protontherapy application [4] (see Fig. 1 and parameters of the ring in Table 1). It is a scale 1 prototype, although the radial extent of its good field region has been reduced by about 40% (from 66.7 cm closed orbit excursion, see Table 1, down to 40 cm) for savings. The general construction specifications are given in Table 2. Figure 2 displays a principle scheme of the yoke, pole and field clamps. Some useful formulae for understanding the various parameters are as follows :

- the spiral *EFB* is defined by $r = r_0 e^{\theta / \tan \zeta}$

- the field satisfies $B(r) = B_0 b_r(r) b_\theta(r, \theta)$ with $b_r(r) = (r/r_0)^k$ obtained from the gap shaping $g(r) \approx g_0(r)(r/r_0)^{-k}$ [1]. The flutter $b_\theta(r, \theta)$ is determined the spiral shape of the *EFB* and by the r-dependent fringe field extent $\lambda(r)$. The latter has been tailored (thanks to the variable chamfer and to the field clamps) so to satisfy as closely as possible $\lambda(r) \propto r$.

Table 1: Parameters of the Spiral Ring

Extraction energy, variable (E_{xtr})	MeV	$70 - 180$
Injection energy, variable (E_{inj})	MeV	$5.55 - 15$
$B\rho_{xtr}/B\rho_{inj}$	T.m	3.612
Number of cells (N)		10
Packing factor (pf)		0.34
Magnet	deg.	see below
r on injection/extraction (r_{inj}/r_0)	m	2.794/3.460
field at r_{inj}/r_0 for $E_{xtr} = 180\,\text{MeV}$	T	0.58/1.70
ν_x		2.76
ν_z for $15 \rightarrow 180\,\text{MeV}$		$1.55 \rightarrow 1.60$

FIELD MEASUREMENTS

All useful details concerning the magnetic field measurements can be found in a companion paper [2], includ-

Table 2: Design Specifications of the Dipole Prototype

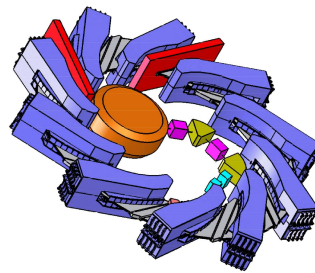| field index (k)		5.00
spiral angle (ζ)	deg.	53.7
sector angle (A)	deg.	12.24
bending angle (β)	deg.	36
radial good field region (GFR)	m	$2.9 < r < 3.3$
Energy range at max. field in GFR	MeV	$23 < E < 106$
vertical good field region	m	$\approx \text{gap}/2$
horizontal tune ν_x		2.76
vertical tune ν_z		$1.56 - 1.59$

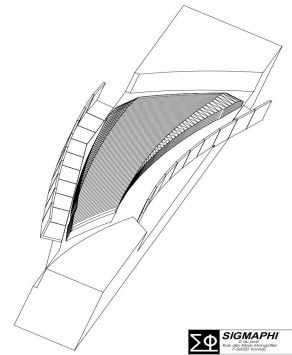Figure 1: A Principle Scheme of the RACCAM Ring, a Variable Energy, Spiral Lattice Proton FFAG.

Figure 2: A scheme of the spiral dipole.

ing evaluation of the parameters introduced above as fringe field extent and r-dependence $\lambda(r)$, the $I_1(r)$ integral, and other field index k, relevant to the determination of the periodic parameters. The mesh size in these measurements was taken rather wide, 11 mm radial and 0.2 degrees azimuthal (referred at machine center), for the essential purpose of limiting the duration of the measurements. It will be seen that, in spite of that, the precision of the tracking is good enough for obtaining major machine parameters as closed orbits, tunes and their evolution with energy, dynamical acceptance, etc. The various aspects of these field measurements relevant to the present work will be addressed in due place.

In the following it will be referred to the "maximal current", $I_{max} = 225$ Amps in the magnet coils, which yields a field value $B_0 = 1.933\,\text{T}^1$ at $r_0 = 3.460\,\text{m}$ (yielding a theoretical 227 MeV top energy)[2], and to the fractional current values at which measurements have been performed, namely, 80% ($B_0 = 1.606\,\text{T}$ measured at r_0, 162 MeV top

---

* SIGMAPHI, Vannes
† CEA & IN2P3, LPSC, UJF-G1, CNRS/IN2P3, INP-G

[1] Actually, extrapolated from 1.7506 T measured at 200 Amps, and accounting for saturation effect.

[2] From, $\rho_0 = r_0 \sin(A/2)/\sin(\beta/2)$, $p = q\,B_0\rho_0$ and $E = (p^2c^2 + M^2c^4)^{1/2} - Mc^2$

energy), and 60% ($B_0 = 1.227$ T measured at r_0, 98 MeV top energy).

TRACKING TOOLS

A number of computing tools, used here, have been developed during the RACCAM study [5, 6], allowing automatic finding of machine parameters from ray-tracing methods and in particular from magnetic field maps, including closed orbits, tunes, maximum stable amplitudes, etc. All are based on the use of the computer code Zgoubi [7].

TRACKING IN 2-D FIELD MAPS

A series of extensive measurements had the goal of systematical exploration of the radial extent of the gap. From these it is possible to assess the periodic parameters, as described hereafter. For that, 2-D field maps at $z = 0$ have been produced, by measuring series of 11 arcs of circles in 5 different regions $r = R \pm 55$ mm, step 11 mm with $R = 2750, 2900, 3125, 3300, 3450$ mm [2]. Prior to launching the data acquisition, it has been controlled that the radial (B_r) and azimuthal (B_θ) components of the field at $z = 0$ are negligible, or made negligible by adjusting the alignment of the measurement plane.

Figure 3 for illustration shows the field in median plane along 5 arcs of circles at $r = 3050, 3070, 3125, 3180, 3200$ mm, maximal current ; the extreme two $B_z(\theta)$ curves at $r = 3050, 3200$ mm, are obtained by extrapolation from the inner, measured ones : it can be observed that overshoots begin to appear, due to the extrapolation off the map and to the presence of slight local inhomogeneities in the measured field, which indicates that trajectory excursions should not overpass too much the measured region, a criterion fulfilled in the following. Figure 4 shows typical field in these conditions on closed orbit, well contained within $r = 3125 \pm 55$ mm.

Closed Orbits

A built-in fitting procedure in Zgoubi is used to ensure that the computed reference closed orbit (fitted by varying the local coordinates and the energy) is contained within ± 55 mm from the reference radius, namely it is requested that the closed orbit in the magnet reaches some value $\hat{r} < R + 55$ mm.

Table 3 summarized the results so obtained, namely, for a closed orbit with peak excursion $\hat{r}$, its energy $E_{c.o.}$, the field $\hat{B}$ experienced at $\hat{r}$. Consistently, the theoretical radius r that the energy $E_{c.o.}$ corresponds to (following $E = (p^2c^2 + M^2c^4)^{1/2} - Mc^2$ with $p = p_0(r/r_0)^{k+1}$) differs by no more than a few per mil from $\hat{r}$.

Tunes

Using the data above the paraxial tunes can be computed from multi-turn tracking and Fourier analysis, for the
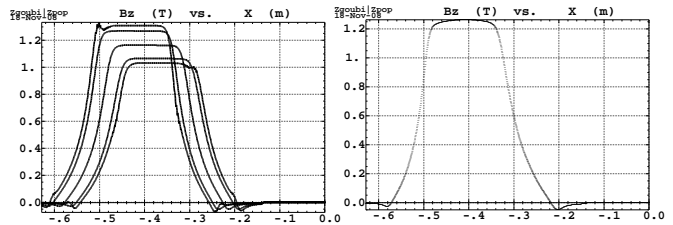

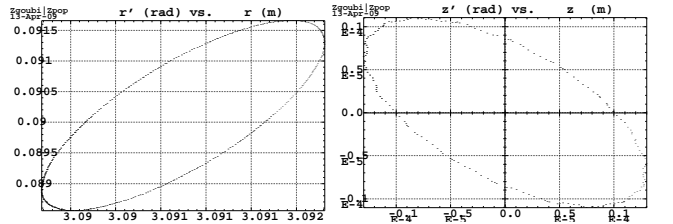Figure 3: Magnetic field along 5 arcs of circles.

Figure 4: Field on closed orbit in the $R = 3125$ mm region.

Figure 5: Typical paraxial motion used for tune computation, horizontal (left), vertical (right).
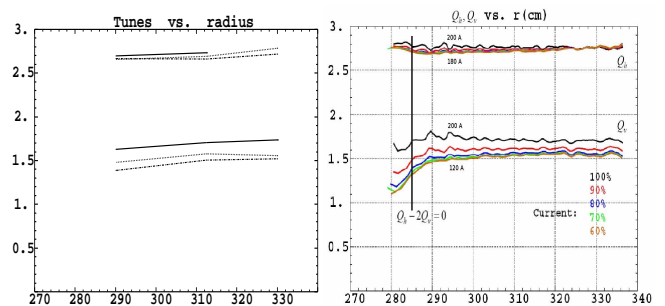

Figure 6: Tunes, form magnetic measurements (left) or magnet simulations (right).

3 ranges $R = 2900, 3125, 3300$ mm within good field region, and for three current values, I_{max}, 80% and 60%. Figure 5 shows typical phase-space plots, for a particle in the $R = 3125$ mm region, 400 cell traversals, and the satisfactory symplecticity of the multiturn ray-tracing (good emittance conservation). So computed tunes are displayed in Fig. 6, together for comparison with those obtained during the magnet design study using OPERA-3D field maps (with $I \approx 200$ A, $B_0 = 1.7$ T at r_0) [5, 1], Global behavior is as expected, weak variation of the horizontal tune with radius and working current ; similar result for the vertical tune in the linear regime $I < 80\%$ of I_{max}, and larger variation beyond. The measurement outcomes, Fig. 6-left, are reasonably close to the simulated behavior, Fig. 6-right. Thorough analysis of these data is being carried on, including comparison with OPERA 3D outcomes, and will be subject to publication in the future.

Dynamic Apertures

2-D field measurements also allow characterizing large amplitude motion, as follows. Figure 7 shows typical hor-

Table 3: Energy on Closed Orbit, Maximum Excursion, Field at Maximum Excursion

R (mm)	$E_{c.o.}$ (MeV)	$\hat{r}$ (mm)	$\hat{B}$ (T)
Maximal current			
2900	38.0	2950	0.880
3125	86.5	3175	1.259
3300	156.0	3350	1.631
$80\%I_{max}$			
2900	26.2	2950	0.719
3125	60.8	3175	1.032
3300	112.7	3350	1.356
$60\%I_{max}$			
2900	15	2950	0.546
3125	35.9	3175	0.782
3300	67.3	3350	1.031

Table 4: Dynamic Apertures

		From measured field maps		From OPERA 3D field maps	
R region (mm)	E (MeV)	Ax	Az	Ax	Az
		(πmm.mrad)			
Maximal current		($B_0 = 1.933\,T$)		($B_0 = 1.7\,T$)	
2900	38.0	1800	900	2500	900
3125	86.5	2600	800	2900	1000
3300	156	5500	1500	3500	950
$80\%I_{max}$		($B_0 = 1.606\,T$)			
2900	15	4000	1500		
3125	35.9	1500	1200		
3300	67.3	1700	1400		
$60\%I_{max}$		($B_0 = 1.227\,T$)			
2900	15	1200	900		
3125	35.9	1200	900		
3300	67.3	2200	900		

izontal motion at maximum stable amplitude (86.5 MeV particle, 1000 cell traversals, including very small vertical emittance to account for possible coupling - the large, outer invariant - or with zero vertical motion - the inner invariant), however an approximate approach of the DA, given the following : during that motion the radial excursion reaches $2993 < r < 3268$ mm, as shown in Fig. 9, somewhat beyond the field map data radial range $3070 < r < 3180$ mm, so that the magnetic field extrapolation from the map as performed by the ray-tracing method reaches validity limits, as observed from the substantial overshoots experienced during extreme radial trajectory excursion, in the $r \approx 3268$ mm region, Fig. 10.

Figure 8 shows typical maximum vertical stable amplitude with horizontal motion launched on closed orbit. The field is computed by second order polynomial extrapolation from the 2-D median plane field map. The field experienced at non-zero z in this motion is free of any noticeable overshoot, an indication that the conditions of field extrapolation are within validity limits.

The dynamic acceptance values so obtained compare reasonably well in magnitude with theoretical DAs obtained from the modelling of the prototype dipole performed for its design study [5, Table 5.5, p. 136] [6]. These results are gathered in Table 4 in the maximal and 60% current cases, calculation of the horizontal DA includes small vertical motion. Data analysis are being carried on and will be subject to future publication.
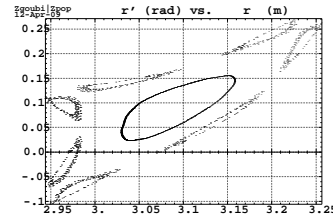

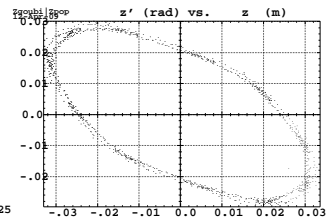Figure 7: Maximum horizontal stable motion, 3125 mm region.

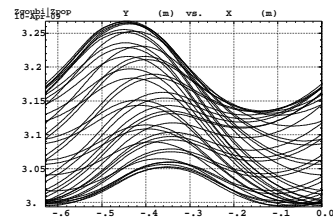Figure 8: Maximum vertical stable motion.

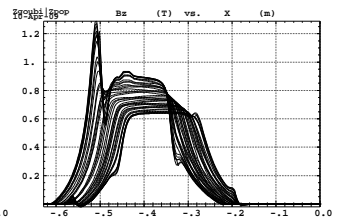Figure 9: Radial trajectory excursion in the con's of Fig. 7.

Figure 10: Magnetic field experienced in the con's of Fig. 7.

TRACKING IN 3-D FIELD MAP

A series of measurements had the goal of evaluating the field behavior off the median plane. For that, a 3-D field map has been produced, by measuring the $z = 0$ plane and the $z = 4$ mm plane fields, in the central region of the magnet, $r \approx 3125$ mm. The $z = -4$ mm 2-D map is generated from the $z = 4$ mm one, by symmetry (regardless of possible vertical inhomogeneities, though). Exploitation of these data for DA computation is underway.

REFERENCES

[1] Design of a prototype gap shaping spiral dipole for a variable energy protontherapy FFAG, T. Planche et al., NIM A 602 (2009) 293305.

[2] Magnetic measurements in a spiral FFAG dipole, M.-J. Leray, these Proceedings.

[3] hhttp://lpsc.in2p3.fr/service_accelerateurs/raccam.htmi

[4] Principle design of a protontherapy, rapid-cycling, variable energy spiral FFAG, S. Antoine et al., NIM A 602 (2009) 293305.

[5] Les accélérateurs à champ fixe et gradient alterné FFAG et leur application médicale en protonthérapie, J. Fourrier, PhD Thesis, LPSC, Grenoble (2008).

[6] Spiral FFAG lattice design tools. Application to 6-D tracking in a proton-therapy class lattice, J. Fourrier et al., NIM A 589 (2008) 133-142.

[7] (a) The ray-tracing code Zgoubi, F. Méot, NIM A 427 (1999) 353-356 ; (b) Zgoubi users' guide, F. Méot, S. Valero, CEA DAPNIA SEA-97-13/FERMILAB-TM-2010 (1997) ;